ELSEVIER

Journal of Chromatography A, 866 (2000) 147–171

JOURNAL OF CHROMATOGRAPHY A

www.elsevier.com/locate/chroma

Kinetic study of the mass transfer of bovine serum albumin in anion-exchange chromatography

Kanji Miyabe[a,b], Georges Guiochon[a,b,*]

[a]*Department of Chemistry, The University of Tennessee, Knoxville, TN 37996-1600, USA*

[b]*Division of Chemical and Analytical Sciences, Oak Ridge National Laboratory, Oak Ridge, TN 37831, USA*

Received 24 June 1999; received in revised form 15 September 1999; accepted 22 October 1999

Abstract

A kinetic study was made on the mass transfer phenomena of bovine serum albumin (BSA) in two different anion-exchange columns (Resource-Q and TSK-GEL-DEAE-5PW). The analysis of the concentration dependence of the lumped mass transfer rate coefficient ($k_{m,L}$) provided the information about the kinetics of the several mass transfer processes in the columns and the anion exchangers, i.e., the axial dispersion, the fluid-to-particle mass transfer, the intraparticle diffusion, and the adsorption/desorption. In the Resource-Q column, the intraparticle diffusion had a dominant contribution to the band broadening compared with those of the other processes. The surface diffusion coefficient (D_s) of BSA showed a positive concentration dependence, by which the linear dependence of $k_{m,L}$ on the BSA concentration seemed to be interpreted. On the other hand, in the TSK-GEL-DEAE-5PW column, the contribution of the adsorption/desorption was also important and almost same as that due to the intraparticle diffusion. There are some differences between the intrinsic properties of the mass transfer kinetics inside the two anion exchangers. It was likely that the positive concentration dependence of D_s was explained by the heterogeneous surface model.

Keywords: Kinetic studies; Mass transfer; Anion exchangers; Diffusion coefficients; Albumin

1. Introduction

Liquid chromatography significantly contributes to the progress of fundamental and applied biochemistry. An immense array of biologically active compounds are currently extracted, separated, and/or purified by preparative liquid chromatography [1,2]. Peptides and proteins are most frequently separated using anion-exchange chromatography [3–6]. A wide variety of packing materials are available for their separation. Numerous publications discuss the physical properties and the characteristics of these materials, the separation mechanisms involved, and the equilibrium thermodynamics of many compounds in these phase systems [7–19]. By contrast, most issues related to the mass transfer kinetics of peptides and proteins in anion-exchange chromatography are still unsolved.

Mass transfer of solutes between the mobile and stationary phases is usually analyzed by assuming that the kinetic process consists of the following three steps, (1) the external mass transfer of the solute molecules from the bulk mobile phase to the

*Corresponding author. University of Tennessee, Department of Chemistry, 611 Buehler Hall, Knoxville, TN 37996-1600, USA. Tel.: +1-423-9740-733; fax: +1-423-9742-667.

E-mail address: guiochon@utk.edu (G. Guiochon)

0021-9673/00/$ – see front matter
PII: S0021-9673(99)01127-9

surface of the packing particles (fluid-to-particle mass transfer); (2) the diffusive transport through the pores of these particles (intraparticle diffusion); and (3) the adsorption/desorption processes at the actual adsorption sites [1]. Axial dispersion and these three mass transfer processes affect the spreading of chromatographic peaks. Axial dispersion and the fluid-to-particle mass transfer resistances are inherent to flow processes in packed beds. The extent of axial dispersion depends on the skill with which homogeneous columns are packed. However, in the separation of macromolecules such as peptides and proteins, the contributions of axial dispersion and the fluid-to-particle mass transfer to band broadening are usually relatively small. By contrast, the kinetic characteristics of intraparticle diffusion and adsorption/desorption are intrinsic properties of the packing materials.

The intrinsic characteristics of the mass transfer kinetics inside particles of the stationary phases must be clarified to evaluate the actual performance of anion-exchange packing materials. Several papers discussed intraparticle diffusion of proteins [8,11,16,18–22]. However, little information was obtained on the possible concentration dependence of the mass transfer kinetic parameters in anion-exchange chromatography. The dependence of both the phase equilibrium and the mass transfer kinetics on the solute concentration is closely related to the separation behavior of nonlinear chromatography.

A series of detailed studies were made on the retention of bovine serum albumin (BSA) in anion-exchange chromatography from the viewpoints of phase equilibrium [23,24] and mass transfer kinetics [25,26]. It was demonstrated that the adsorption equilibrium could be well accounted for by the modified bi-Langmuir isotherm and that the lumped mass transfer rate coefficient, $k_{m,L}$ (based on an adsorbed-phase driving force) increased linearly with increasing concentration of BSA. The value of $k_{m,L}$ was determined from breakthrough curves by applying the shock layer theory, in which the mass transfer kinetics is accounted for by the lumped kinetic model (solid film linear driving force model) [1]. In a previous paper [27], we analyzed the concentration dependence of $k_{m,L}$ and obtained detailed information concerning the mass transfer kinetics of the four transport processes in the column, (1) axial dispersion, (2) the fluid-to-particle mass transfer, (3) intraparticle diffusion, and (4) adsorption/desorption.

Surface diffusion had a significant influence on the characteristics of the mass transfer of BSA. The linear concentration dependence of $k_{m,L}$ results probably from that of the surface diffusion coefficient (D_s). The positive dependence of D_s of BSA on the concentration could be interpreted by the heterogeneous surface model, suggesting that there is a distribution of the adsorption energy on the surface of the anion exchanger. A similar positive concentration dependence was demonstrated for the mass transfer rate coefficient (k_m) in the elution of Tröger's base on microcrystalline cellulose triacetate [28,29], and for $k_{m,L}$ in the enantiomeric separation of D- and L-phenylalanine anilide on a polymeric imprinted stationary phase [30]. A few other papers describe the concentration dependence of intraparticle diffusivity [31,32], of axial dispersion in size exclusion chromatography [33], of the effective diffusivity of a small molecular mass protein in bulk solutions [34], and of the mutual diffusion coefficient of a macromolecular protein (globular protein ovalbumin) [35].

The goal of this work is to derive relevant information on the actual mass transfer kinetics of BSA in two different anion-exchange columns (Resource-Q and TSK-GEL-DEAE-5PW) and to compare the intrinsic characteristics of the mass transfer kinetics in these two anion exchangers. It also attempts to explain the positive concentration dependence of D_s.

2. Theory

Various theories and models were suggested to account for phase equilibrium thermodynamics and mass transfer kinetics in liquid chromatography [1,36]. In this study, we used the modified bi-Langmuir isotherm to represent the adsorption equilibrium and the lumped kinetic model for the mass transfer kinetics of BSA in anion-exchange chromatography. The required details can be found in the original papers [25,26] and in the literature cited [1].

2.1. Adsorption equilibrium

The experimental data characterizing the adsorp-

tion equilibrium of BSA in the two phase systems studied, using two different anion-exchange packing materials, were represented by the modified bi-Langmuir isotherm [1,23–26,36].

$$q = \frac{a_1 C}{1 + b_1 C} + a_2 C \tag{1}$$

where C and q are the concentration of BSA in the mobile and the stationary phases, respectively, and a_1, b_1, and a_2 are numerical parameters, all independent of C. It was experimentally confirmed that the term $b_2 C$ was negligible compared to unity.

2.2. Mass transfer kinetics

In this study, the concentration dependence of $k_{m,L}$ was determined from the experimental breakthrough curves which were analyzed by using an equation (described later), in which $k_{m,L}$ was assumed to be related to the contributions of the different mass transfer processes in the column.

2.2.1. The general kinetic model in chromatography

The general kinetic model of chromatography is a complete model which considers three phases, that is, (1) the bulk mobile phase percolating through the bed of particles, (2) the mobile phase stagnant inside the porous particles, and (3) the stationary phase. The set of equations of this model includes the mass balance equations of the compound in the column and in the particles, and the kinetic equations describing the mass transfer between the phases. They are written as follows [1].

$$u \cdot \frac{\partial C}{\partial z} + \frac{\partial C}{\partial t} + F \cdot \frac{\partial q_{av}}{\partial t} = D_L \cdot \frac{\partial^2 C}{\partial z^2} \tag{2}$$

$$q_{av} = \frac{3}{R_p^3} \int_0^{R_p} r^2 q \mathrm{d}r \tag{3}$$

$$M_F = D_e \cdot \left.\frac{\partial C_p}{\partial r}\right|_{r=R_p} = K_f \left(C - C_p|_{r=R_p}\right) \tag{4}$$

$$\epsilon_p \cdot \frac{\partial C_p}{\partial t} + (1 - \epsilon_p) \cdot \frac{\partial C_s}{\partial t} = D_e \cdot \left(\frac{\partial^2 C_s}{\partial r^2} + \frac{2}{r} \cdot \frac{\partial C_p}{\partial r}\right) \tag{5}$$

$$\left.\frac{\partial C_p}{\partial r}\right|_{r=0} = 0 \tag{6}$$

$$\frac{\partial C_s}{\partial t} = k_{ads} \cdot (C_p - C_p^*) = k_{ads} \cdot \left(C_p - \frac{C_s}{K_a}\right) \tag{7}$$

where q_{av} is the solute concentration in the stationary phase (q) averaged over the entire particle, F the phase ratio [$F = (1 - \epsilon_T)/\epsilon_T$, with ϵ_T, the total column porosity], u the average interstitial velocity of the mobile phase, t the time, z the longitudinal distance along the column, D_L the axial dispersion coefficient, R_p the particle radius, r the radial distance from the center of the particle, M_F the mass flux of the solute from the bulk solution to the external surface of the stationary phase particle, D_e the intraparticle diffusivity, C_p the concentration of the solute within the pores inside the particle, k_f the external mass transfer coefficient, ϵ_p the internal porosity of the particle, C_s the concentration of the solute adsorbed on the stationary phase, k_{ads} the adsorption rate constant, C_p^* the value of C_p when the system is in equilibrium with a stationary phase concentration C_s, and K_a the adsorption equilibrium constant. The initial and boundary conditions are as follows.

$$C(z,0) = 0 \tag{8a}$$

$$C_p(r,z,0) = 0 \tag{8b}$$

$$C(0,t) = C_0 \quad \text{for } 0 \le t \le t_p \tag{8c}$$

$$C(0,t) = 0 \quad \text{for } t \ge t_p \tag{8d}$$

where t_p and C_0 are the width and the height of the rectangular injection pulse, respectively. The height equivalent to a theoretical plate, HETP (H) in linear chromatography can be derived from the first and the second moments of the solution of the general kinetic model.

$$H = \frac{2D_L}{u} + 2 \cdot \left(\frac{k_1}{1 + k_1}\right)^2 \cdot \left[\frac{u d_p}{6 F k_f} + \frac{u d_p^2}{60 F D_e} + \left(\frac{k_p}{1 + k_p}\right)^2 \cdot \frac{u}{F k_{ads}}\right] \tag{9}$$

with

$$k_1 = F\left[\epsilon_p (1 - \epsilon_p) K_a\right] \tag{9a}$$

$$k_2 = \frac{1-\epsilon_p}{\epsilon_p} \cdot K_a \tag{9b}$$

where d_p is the particle diameter.

2.2.2. The lumped kinetic model in linear chromatography

If one of the contributions to the mass transfer kinetics dominates, the chromatographic process is more simply and conveniently represented by the lumped kinetic model [1]. The mass transfer rate is summarily expressed as Eq. (11) which introduces the mass transfer rate coefficient (k_m).

$$\frac{\partial C}{\partial t} + F \cdot \frac{\partial C_s}{\partial t} + u \cdot \frac{\partial C}{\partial z} = D_L \cdot \frac{\partial^2 C}{\partial z^2} \tag{10}$$

$$\frac{\partial C_s}{\partial t} = k_m (C_s^* - C_s) \tag{11}$$

where C_s is the concentration of the solute in the stationary phase, C_s^* the concentration in the stationary phase in equilibrium with the mobile phase concentration C. Eq. (11) assumes that the driving force of the mass transfer is the difference between C_s^* and C_s and that the mass transfer rate is proportional to the driving force. van Deemter et al. [37] derived the following HETP equation in linear chromatography from the analytical solution of Eqs. (10) and (11) proposed by Lapidus and Amundson [38].

$$H = \frac{2D_L}{u} + 2 \cdot \left(\frac{k_0'}{1+k_0'}\right)^2 \cdot \frac{u}{k_0' k_m} \tag{12}$$

where k_0' is the retention factor at infinite dilution. The comparison of Eqs. (9) and (12) gives

$$\frac{F}{k_0' k_m} = \frac{d_p}{6k_f} + \frac{d_p^2}{60D_e} + \left(\frac{k_p}{1+k_p}\right)^2 \cdot \frac{1}{k_{ads}} \tag{13}$$

Eq. (13) shows that the mass transfer coefficient in the solid film linear driving force model (k_m) is related to the three kinetic parameters, the external mass transfer coefficient (k_f), the intraparticle diffusivity (D_e), and the adsorption rate constant (k_{ads}), and that the contributions due to the three mass transfer processes are additive.

2.2.3. An HETP equation for nonlinear chromatography

The following HETP equation, similar to Eq. (12), was derived from the shock layer theory in frontal analysis, under constant pattern behavior. It is valid in nonlinear chromatography, at least as long as the column efficiency is not very low [1].

$$H = \frac{2D_L}{u} + 2 \cdot \left(\frac{K}{1+K}\right)^2 \cdot \frac{u}{K k_m} \tag{14}$$

where K is the slope of the isotherm chord [$K = FK_a = F(\Delta q/\Delta C)$]. So, k_0' in Eq. (12) is replaced by K in Eq. (14). This equation proves that the contributions of axial dispersion and the mass transfer processes are additive in nonlinear chromatography as well as in linear chromatography, at least in frontal analysis, under constant pattern behavior, and assuming the solid film linear driving force model. The contributions of each mass transfer process in nonlinear frontal analysis, (1) the fluid-to-particle mass transfer, (2) intraparticle diffusion, and (3) the adsorption/desorption kinetics are summarized into a single kinetic parameter, k_m. The value of D_L in Eq. (10) is probably negligible in the separation of proteins [25,26] and it can be taken as zero. Even though the contribution of axial dispersion cannot be completely neglected, k_m in Eq. (11) suffices to represent it. In this paper, we analyze the lumped mass transfer rate coefficient ($k_{m,L}$), with which the contribution of axial dispersion is lumped. The value of $k_{m,L}$ is probably comparable to that of k_m because the contribution of axial dispersion is predicted to be small compared with those of the other mass transfer processes in the separation of macromolecules.

Eq. (13) proves theoretically that the contributions of the different mass transfer processes are additive in linear and locally linear chromatography. In nonlinear chromatography, however, there are no equations correlating k_m and the different mass transfer kinetic parameters, k_f, D_e and k_{ads}. In this study, an attempt was made to evaluate the individual contributions of the mass transfer processes to the separation efficiency by assuming the following equation, similar to Eq. (13).

$$\frac{F}{K k_m} = \frac{d_p}{6k_f} + \frac{d_p^2}{60D_e} + \left(\frac{k_p}{1+k_p}\right)^2 \cdot \frac{1}{k_{ads}} \tag{15}$$

The applicability of Eq. (15) will be checked later by comparing the calculation results obtained in this study with those reported in other publications.

In this study, we assumed that intraparticle diffusion arises from the parallel contributions of pore and surface diffusion [39,40].

$$D_e = D_p + (1 - \epsilon_p)K_a D_s \quad (16)$$

where D_p and D_s are the pore diffusivity and the surface diffusion coefficient, respectively. Eq. (16) is valid under linear isotherm conditions. The following equation was used for correlating D_p with the molecular diffusivity (D_m) [1].

$$D_p = \left(\frac{\epsilon_p}{2 - \epsilon_p}\right)^2 \cdot D_m \quad (17)$$

3. Experimental

In this work, we reevaluated in more detail previous experimental data on phase equilibrium and mass transfer kinetics obtained in anion-exchange chromatography with BSA as probe compound [25,26]. We supply here only the information on the experimental conditions which is necessary to understand the analytical results derived in this paper. Other details on the experimental work can be found in the original papers [25,26].

3.1. Chromatographic conditions

Two different anion-exchange columns were used.

(a) A 3 cm×0.64 cm stainless steel column (No. 17-1177-01) packed with Pharmacia Resource-Q (d_p, 15 μm; pore size, 200–10 000 Å), with a hold-up volume (V_0) of 0.750 ml, a stationary phase inaccessible volume (V_a) of 0.215 ml, and an efficiency (N) of 400 plates for uracil (unretained) in 25 m*M* Bis-Tris–HCl buffer (pH 6.0) at the flow-rate of 1 ml min^{-1}. The total porosity (ϵ_T) of the column was calculated as 0.777 and the phase ratio (F) as 0.287.

(b) A 7.5 cm×0.75 cm stainless steel column (No. S0116) packed with TSK-GEL-DEAE-5PW (d_p, 10 μm; pore size, 1000 Å), with V_0 of 2.58 ml, V_a of 0.73 ml and N=2800 plates for cytidine-5′-monophosphate (unretained) at the flow-rate of 1 ml min^{-1} of an eluent containing 35 m*M* NaCl in 20 m*M* Tris–HCl buffer (pH 8.0). The values of ϵ_T and F are calculated as 0.780 and 0.282, respectively.

The mobile phase was the buffer solutions, which were prepared by dissolving 25 m*M* Bis-Tris or 50 m*M* Tris in water and titrating with HCl until pH 6.0. The sample solutions were prepared by dissolving known amounts of BSA in the buffer solutions.

3.2. Procedures

After the completion of each experiment, the necessary regeneration procedures (i.e., cleaning or defouling) of the stationary phase were undertaken, followed by the equilibration of the phase system. Then, a new buffer solution of BSA was pumped into the columns until it broke through. A series of single step breakthrough curves were measured, in the order of increasing BSA concentration step. The measurement of the breakthrough curves was made at the flow-rate of 1 ml min^{-1}. Each breakthrough curve gives one data point of the equilibrium isotherm. The isotherm data were fitted to the modified bi-Langmuir model (Eq. (1)). From the equilibrium isotherm, the breakthrough curves were calculated for each concentration step using different constant $k_{m,L}$ values. This coefficient was kept constant during any such calculation. The experimental breakthrough curves were compared to the calculated ones. The rate coefficient for which there was the best agreement between experimental and calculated breakthrough curves was taken as the best value of $k_{m,L}$ for the average concentration of the concentration step.

4. Results and discussion

We will compare the mass transfer kinetics properties of two anion-exchange packing materials. First, kinetic parameters related to the mass transport processes in the columns were derived from an analysis of the experimental results concerning phase equilibrium and mass transfer kinetics determined from the breakthrough curves in single step frontal analysis [25,26]. Second, the contributions of each mass transport process to band broadening were individually evaluated and compared with each other. Finally, an attempt was made to explain the

concentration dependence of D_s by applying different models.

4.1. Adsorption equilibrium

Fig. 1 shows the equilibrium isotherms of BSA on the two columns. The experimental data were well represented by the modified bi-Langmuir isotherm (Eq. (1)) rather than by a simple Langmuir isotherm [23–26]. Table 1 shows the best values of the numerical parameters, a_1, b_1 and a_2. Although Eq. (1) contains only three parameters, the isotherm data of BSA on both anion exchangers were well accounted for. The amount adsorbed (q) at equilibrium with a given mobile phase concentration (C) is larger for Resource-Q than for TSK. However, the same dependence was observed in both phase systems. The steep rise of q in the low concentration range corresponds to the first term in the right-hand-side (RHS) of Eq. (1). The contribution of this term saturates rapidly between $C=0.5$ and 1.0 mg ml^{-1}. Then, q increases linearly with increasing C for C larger than about 0.5–1.0 mg ml^{-1}. The subsequent increase in q arises from the second term in the RHS of Eq. (1). The physical interpretation of this model is that the isotherm is probably a bi-Langmuir model but that the coefficient b_2 is too small to be measured and b_2C is negligible in the range of concentrations accessible experimentally.

Table 1
Parameters of the equilibrium isotherm and the mass transfer kinetics

	Column	
	Resource-Q	TSK-GEL-DEAE-5PW
a_1 (–)	4906.7	1380.5
b_1 (ml mg^{-1})	35.75	17.32
a_2 (–)	14.97	11.94
$k^0_{m,L}$ (s^{-1})	$1.6\cdot10^{-3}$	$5.8\cdot10^{-4}$
$k^1_{m,L}$ (ml mg^{-1} s^{-1})	$3.290\cdot10^{-2}$	$9.93\cdot10^{-3}$

The satisfactory description of the equilibrium isotherm data by the modified bi-Langmuir equation is no proof of the existence of two types of interactions with different energies between the BSA molecules and the surface of the anion exchangers [23–26]. The surface of these exchangers is probably heterogeneous, with many different adsorption sites and a wide adsorption energy distribution. The

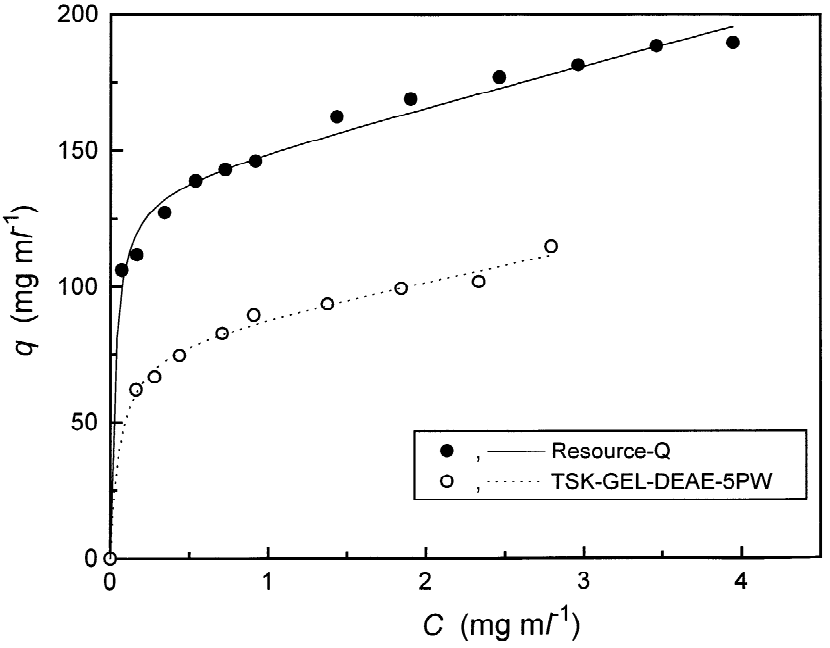

Fig. 1. Experimental isotherm data (plots) and best fit bi-Langmuir isotherm (lines) of BSA.

presence of more complicated interactions between the BSA molecules and these adsorption sites may be anticipated.

4.2. Mass transfer rate coefficient

As described originally [25,26], the lumped mass transfer rate coefficient ($k_{m,L}$) determined from the breakthrough curves includes the contribution of axial dispersion to band broadening. The HETP is related to the Stanton number (St) as follows.

$$H = \frac{K}{(1+K)^2} \cdot \frac{2L}{\mathrm{St}} \tag{18}$$

with

$$\mathrm{St} = \frac{k_{m,L} L}{u} \tag{18a}$$

where L is the column length. Comparing Eqs. (14) and (18) gives

$$\frac{1}{K k_{m,L}} = \left(\frac{1+K}{K}\right)^2 \cdot \frac{D_L}{u^2} + \frac{1}{K k_m} \tag{19}$$

Then, combining Eqs. (15) and (19) gives

$$\frac{F}{K k_{m,L}} = \left(\frac{1+K}{K}\right)^2 \cdot \frac{F D_L}{u^2} + \frac{d_p}{6 k_f} + \frac{d_p^2}{60 D_e} + \left(\frac{k_p}{1+k_p}\right)^2 \cdot \frac{1}{k_{ads}} \tag{20}$$

Eq. (20) explains how the parameter $k_{m,L}$ correlates with the individual contributions of the four basic mass transfer processes in the column.

Fig. 2 illustrates the linear dependence of $k_{m,L}$ on the concentration of BSA, calculated as the average of the concentration step in frontal analysis. The solid and dotted lines represent the results of the two linear regressions of the experimental data [25,26].

$$k_{m,L} = k^0_{m,L} + k^1_{m,L} C \tag{21}$$

Table 1 also lists $k^0_{m,L}$ and $k^1_{m,L}$. As indicated in the original papers [25,26], $k_{m,L}$ was estimated by fitting the calculated breakthrough curve to the experimental one. The precision of the determination of $k_{m,L}$ was estimated to be about ±10%. Also, in the calculations made to estimate $k_{m,L}$, the whole set

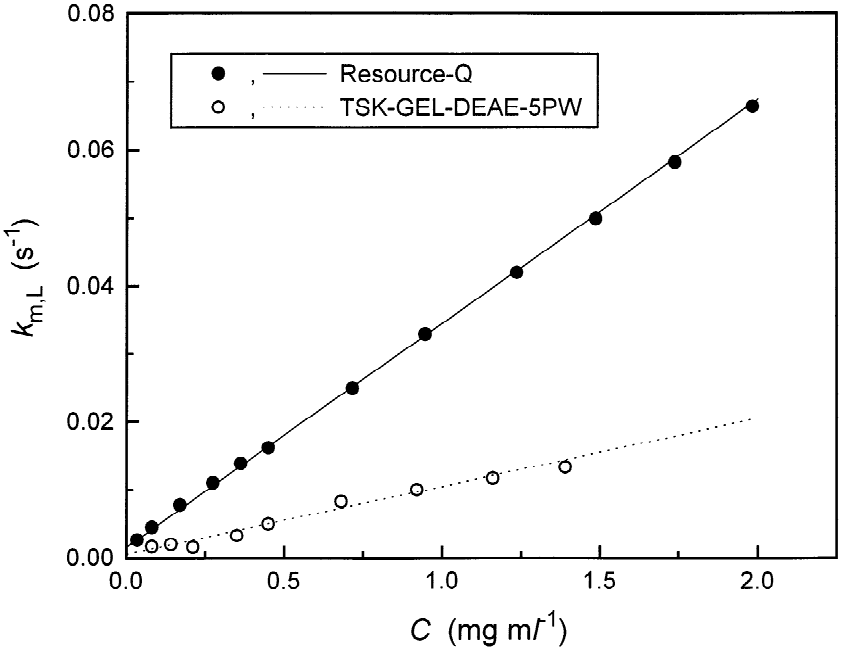

Fig. 2. Dependence of $k_{m,L}$ on the BSA concentration.

of experimental data points was shifted by no more than a few percent in order to adjust the mass centers of the experimental and the calculated breakthrough curves. This suggests that the equilibrium data were determined with an error of a few percent.

The experimental values of St for BSA range from 0.12 to 3.0 on the Resource-Q column (u, 0.067 cm s^{-1}; L, 3 cm; $k_{m,L}$, $2.7\cdot10^{-3}$–$6.6\cdot10^{-2}$ s^{-1}) and from 0.26 to 2.1 on the TSK column (u, 0.048 cm s^{-1}; L, 7.5 cm; $k_{m,L}$, $1.7\cdot10^{-3}$–$1.3\cdot10^{-2}$ s^{-1}). As explained earlier, the column efficiencies for unretained compounds were measured at 400 (Resource-Q column) and 2800 plates (TSK column). At $C=$ 1.0 mg ml^{-1}, the intermediate concentration of the plots in Fig. 2, K is calculated as between 20 and 30 from Fig. 1 or from the isotherm parameters in Table 1. In this case ($K=25$), St is calculated as between 30 and 210 for the Resource-Q and TSK columns, using Eq. (18). Compared with these hypothetical values, the St values reported above are very low. They suggest that the intrinsic properties of the kinetic processes taking place inside the particles of anion exchangers (intraparticle diffusion and/or adsorption/desorption kinetics) have a significant influence on band broadening because axial dispersion and fluid-to-particle mass transfer are expected to have small contributions, as shown previously [27]. As illustrated in Fig. 2, the values of $k_{m,L}$ are larger for the Resource-Q than for the TSK column, by a factor of nearly 3. By contrast, as described above, the column efficiency measured with an unretained compound is 2.8-times higher for the TSK ($N=2800/7.5$ cm) than for the Resource-Q ($N=400/3$ cm) column. Thus, the mass transfer resistance inside the packing materials must be larger for the TSK than for the Resource-Q column. The contributions of each term in Eq. (20) to $k_{m,L}$ must be evaluated individually to clarify the intrinsic kinetic properties of the two anion exchangers in the separation of BSA.

4.3. Estimation of kinetic parameters

Eq. (20) suggests that when K becomes infinite, $F/(Kk_{m,L})$ tends toward the sum of three terms, (FD_L/u^2), $(d_p/6k_f)$ and $(1/k_{ads})$, because, then, the two coefficients $[(1+K)/K]^2$ and $[k_p/(1+k_p)]^2$ become unity. According to Eq. (16), D_e becomes infinite with K. In such a case, the third term in the RHS of Eq. (20) may be neglected. Fig. 3 illustrates the plot of $F/(Kk_{m,L})$ against $1/K$. The solid lines were calculated from the parameters of the isotherm and the mass transfer kinetics listed in Table 1. From the intercepts of the lines in Fig. 3, the sums $(FD_L/u^2)+(d_p/6k_f)+(1/k_{ads})$ are estimated at 0.093 for the Resource-Q column and 0.84 for the TSK column. As described earlier, the errors made in the estimation of $k_{m,L}$ and of the isotherm data were about ±10% and a few percent, respectively. It seems that the intercepts in Fig. 3 also include an error of about ±10%. These values are relatively small compared with those of $F/(Kk_{m,L})$ experimentally measured, i.e., 0.25–0.38 (Resource-Q column) and 1.6–2.1 (TSK column). The value for the TSK column is about one-order of magnitude larger than that for the Resource-Q one, suggesting that there are important differences between the intrinsic kinetic properties of the two anion exchangers.

The value of k_{ads} was estimated by subtracting the contributions of the two terms (FD_L/u^2) and $(d_p/6k_f)$ from the sums. k_{ads} was assumed to be independent of C.

The value of the first term, i.e., FD_L/u^2, can be estimated from the HETP measured for an unretained compound. At $K_a=0$, Eq. (9) can be written as follows.

$$H=\frac{2D_L}{u}+2\cdot\left(\frac{F\epsilon_p}{1+F\epsilon_p}\right)^2\cdot\left[\frac{ud_p}{6Fk_f}+\frac{ud_p^2}{60FD_p}\right] \tag{22}$$

Eq. (22) includes three kinetic parameters, i.e., D_L, k_f, and D_p. The last two parameters can be estimated from various correlations [1,39,40]. We used the Wilson–Geankopolis equation [41].

$$\mathrm{Sh}=\frac{1.09}{\epsilon}\cdot\mathrm{Sc}^{1/3}\mathrm{Re}^{1/3}\ (0.0015<\mathrm{Re}<55) \tag{23}$$

The values of D_p for uracil and cytidine-5′-monophosphate were derived from Eq. (17). The molecular diffusivity (D_m) was estimated from the Wilke–Chang equation [1,42,43].

$$D_{m,s}=7.4\cdot10^{-8}\cdot\frac{(\alpha_{A,sv}M_{sv})^{1/2}T}{\eta_{sv}V_{b,s}^{0.6}} \tag{24}$$

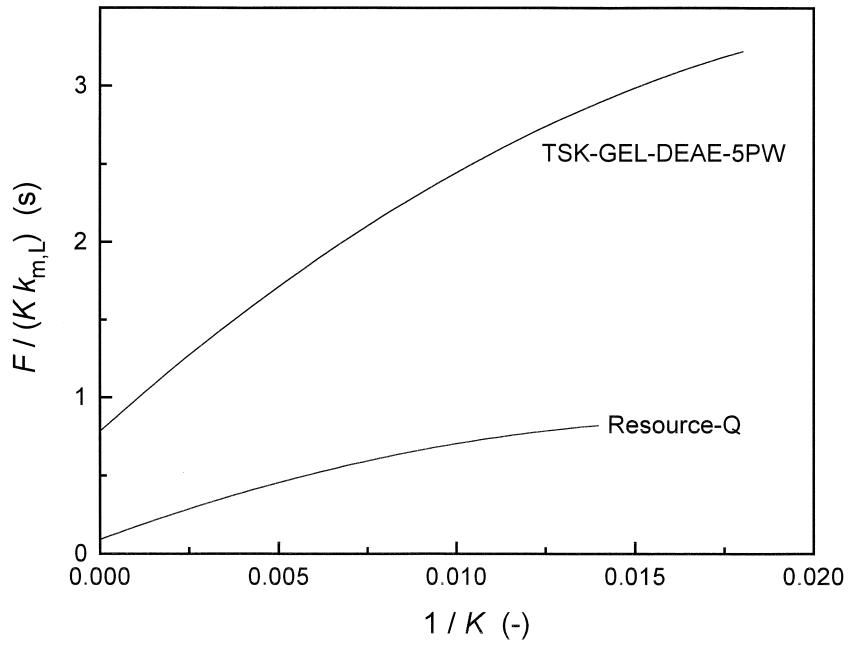

Fig. 3. Correlation between $F/(Kk_{m,L})$ with $1/K$ for the estimation of k_{ads}.

where the subscripts s and sv denote the unretained compound and the solvent, respectively, α_A the association coefficient, M the molecular mass, η the viscosity, T the absolute temperature, and V_b the molar volume at the normal boiling point. Other parameters in Eq. (22) are physical properties of the packing materials and the operational conditions.

For the Resource-Q column, the value of $2D_L/u$ was calculated as $6.5\cdot10^{-3}$ cm from the HETP for uracil measured at a flow-rate of 1 ml min^{-1}. As a consequence, FD_L/u^2 was estimated as $2.7\cdot10^{-2}$ s. Similarly, for the TSK column, the values of $2D_L/u$ and FD_L/u^2 were calculated as $2.3\cdot10^{-3}$ cm and $7.3\cdot10^{-3}$ s, respectively, from the HETP for cytidine-5′-monophosphate at 1 ml min^{-1}. As expected, since the column efficiency was measured with an unretained compound, the contribution of axial dispersion to band broadening is smaller for the TSK than for the Resource-Q column. From the value of D_L/u obtained above, numerical values of 0.46 and 0.87 were derived for ud_p/D_L in the Resource-Q and the TSK column, respectively. It is well known that the ratio ud_p/D_L ranges between 0.5 and 1.0 in liquid–solid systems [40]. The calculated values are thus in agreement with this previous observation, suggesting that the values of D_L obtained in this study are reasonable and probably valid. The value of D_L/u was assumed to be constant, irrespective of the nature of the solute (the unretained compound and BSA) and of the BSA concentration in the sample solutions. This assumption, however, has little influence on the conclusion of this study because the contribution of axial dispersion is so small.

Second, the value of the second term, $d_p/(6k_f)$, was estimated from Eq. (23). The value of D_m for BSA was estimated using the following equation proposed by Guiochon et al. [1].

$$D_{m,B} = 8.31\cdot10^{-8}\cdot\frac{T}{\eta_{sv}M_B^{1/3}} \quad (25)$$

where the subscript B represents BSA. The value of $D_{m,B}$ at 293 K was estimated as $6.0\cdot10^{-7}$ cm^2 s^{-1}, in good agreement with previous experimental data [44]. At a flow-rate of 1 ml min^{-1}, the values of $d_p/(6k_f)$ for BSA were calculated as $3.4\cdot10^{-2}$ s on the Resource-Q column and $4.0\cdot10^{-2}$ s on the TSK column. Although they are of the same order of magnitude, these two contributions to the BSA band

spreading are different. The ratios of $d_p/(6k_f)$ to the experimental value of $F/(Kk_{m,L})$ are ca. 10% and 2% for the Resource-Q and the TSK column, respectively. This shows that the contribution of the mass transfer resistance inside the anion exchanger particles to band broadening is larger in the TSK than in the Resource-Q column. In our work, the concentration of BSA was increased up to 2 mg ml^{-1} (0.2%). However, the concentration dependence of D_m was not taken into account because experimental results suggested that the concentration dependence of D_m was small in the concentration range 0–5% [1]. The dependence of k_f on the BSA concentration was not considered either. These assumptions have little influence on the our calculation results because the contribution of the fluid-to-particle mass transfer to peak broadening is also relatively small, as described above.

In these calculations, the values of the terms FD_L/u^2 and $d_p/(6k_f)$ for BSA were estimated by using some literature correlations in order to derive k_{ads}. The small contributions of axial dispersion and fluid-to-particle mass transfer to band broadening suggest that the estimation error of the related kinetic parameters has a small influence on the precision of k_{ads} and that correct values of k_{ads} were derived, 31 s^{-1} for the Resource-Q column and 1.3 s^{-1} for the TSK column. As described earlier, the intercept in Fig. 3, i.e., the sum of the three terms, $(FD_L/u^2) + (d_p/6k_f) + (1/k_{ads})$, is calculated with an error of about ±10% from the experimental data illustrated in Figs. 1 and 2. The values of k_{ads} derived from there are in error by nearly the same factor. The value of k_{ads} is about one-order of magnitude smaller on the TSK than on the Resource-Q column. This is one of the causes of the smaller value of $k_{m,L}$ on the TSK column (Fig. 2). An appropriate interpretation cannot be provided at this stage because of this difference between the k_{ads} values. This difference is most probably explained by the dissimilarities between the functional ligands, e.g., type, structure and density, of the two packing materials. A more detailed analysis of the adsorption/desorption process at the actual adsorption sites is now required.

The value of D_e at different BSA concentrations can be calculated from Eq. (20) because the contributions of the three mass transfer processes other than intraparticle diffusion can be estimated. As explained earlier, appropriate values of D_L/u were derived for the Resource-Q and the TSK columns. The value of k_f was estimated with an adequate accuracy using the literature correlation, Eq. (23). The error on k_{ads} is estimated at ±10%. In the case of the Resource-Q column, however, the contributions to band broadening of the three mass transfer processes other than intraparticle diffusion are relatively small as shown later. The values of the errors made on D_L, k_f and k_{ads} have little influence on that made on D_e. Rather, the accuracy of the estimation of D_e seems to depend almost only on that of the HETP. As shown in Eqs. (18) and (18a), the error made on H is almost the same as on $k_{m,L}$, probably ±10%. Therefore, it is likely that D_e was estimated with an error of about ±10% for the Resource-Q column. On the other hand, both intraparticle diffusion and the adsorption/desorption process have large contributions to peak spreading in the TSK column. The magnitude of the two contributions is similar. By contrast, the contributions of axial dispersion and fluid-to-particle mass transfer are quite small (see later). The error made on D_e can be estimated to a maximum of ±10% for the TSK column. Although the errors on H and k_{ads} are both estimated at about ±10%, they vary in the same direction.

In Fig. 4a and b, D_e thus calculated is plotted versus C. Although the data points are somewhat scattered in Fig. 4b, similar profiles are observed in both figures. The values of D_e depend on the concentration, because K_a and D_s do too, as shown by Eq. (16). They range from $1.3\cdot10^{-7}$ to $2.4\cdot10^{-7}$ cm^2 s^{-1} on the Resource-Q column and from $1.3\cdot10^{-8}$ to $2.3\cdot10^{-8}$ cm^2 s^{-1} on the TSK column. The ratio D_e/D_m for BSA is between 1/40 and 1/3. The difference between the D_e values is probably associated with differences in pore structure of the two packing materials. As described earlier, the values of ϵ_T and F are almost the same for the two columns. However, the ranges of pore diameters are different. Although the validity of the D_e values derived in this study seems to be confirmed as explained below, further studies on the mass transfer kinetics in anion exchangers should be made to clarify these issues.

Some experimental values of D_e are reported in the literature for macromolecules in porous materials. Graham and Fook [8] studied the equilibrium

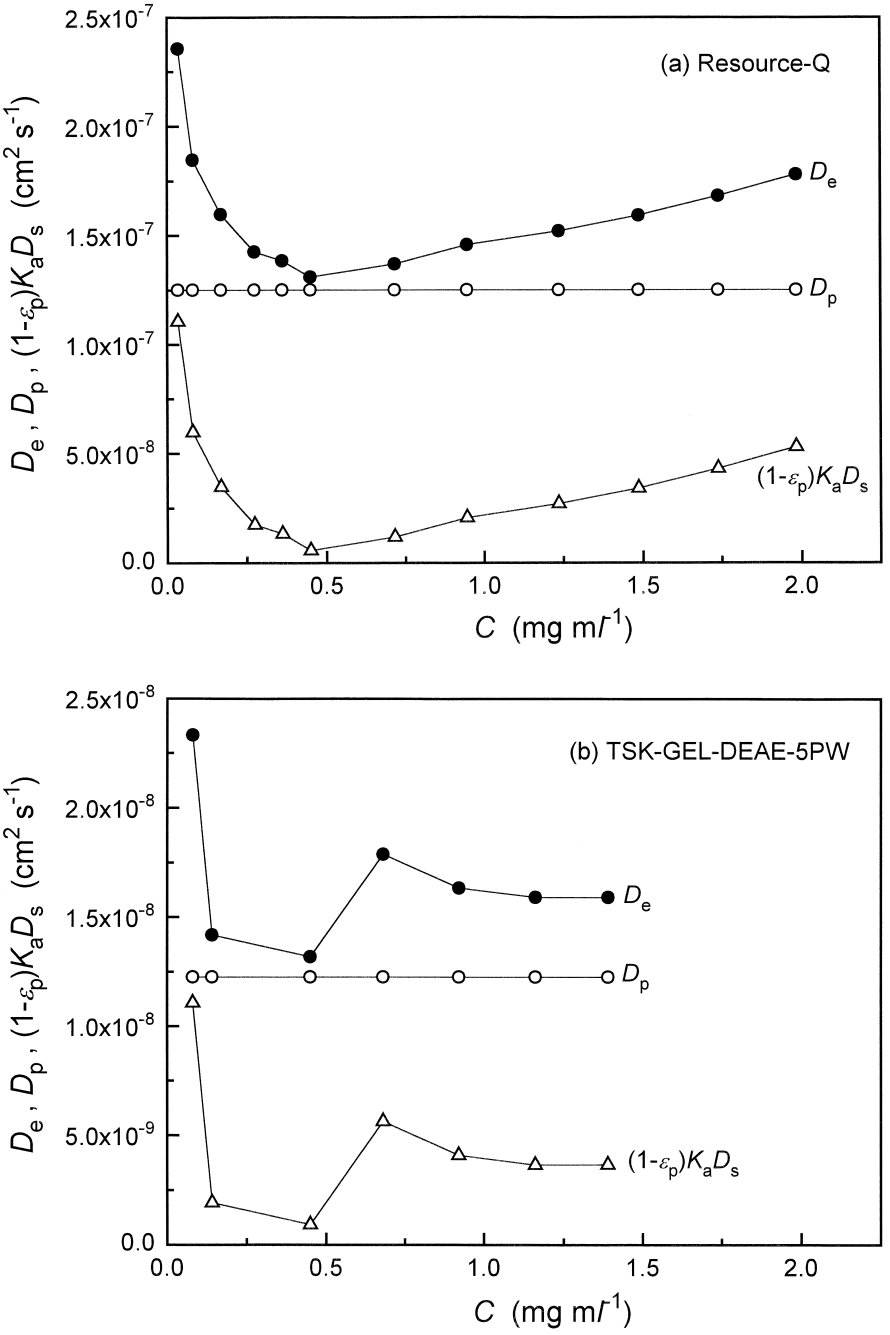

Fig. 4. Comparison of the contributions of the pore and the surface diffusion to the intraparticle diffusion. (a) Resource-Q, (b) TSK-GEL-DEAE-5PW.

and the kinetics of the adsorption of BSA on a DEAE-resin by a batch method. They reported that the diffusion coefficient in the resin was about 100 times smaller than that in the free solution. Similarly, Tsou and Graham [11] reported a calculated effective particle diffusivity of BSA in DEAE-Sephadex A-50 about 20-times smaller than the free diffusivity. Colton et al. [20] reported that D_e/D_m for cytochrome *c* and human hemoglobin on finely porous glass was between 1/10 and 1/3. Skidmore et al. [21] studied the equilibrium and kinetic characteristics of the adsorption of BSA and lysozyme on the strong cation exchanger S Sepharose FF and reported D_e values of $8.5\cdot10^{-8}$ cm^2 s^{-1} and $5.0\cdot10^{-7}$ cm^2 s^{-1} for BSA and lysozyme, respectively. Park et al. [22] reported values of D_e of about $1.8\cdot10^{-7}$ cm^2 s^{-1} for the intraparticle diffusion of BSA labeled with *p*-(isothiocyanato)azobenzene in polyacrylamide gel. Fernandez and Carta [18] and Fernandez et al. [19] reported $9.2\cdot10^{-9}$ cm^2 s^{-1} as the intraparticle BSA diffusivity, value obtained in the assumption that the driving force for the diffusion in composite silica–polyacrylamide gel anion exchangers is the total BSA concentration. Yoshida et al. [16] investigated the mass transfer of BSA on a strongly basic adsorbent, chitosan, using the shallow bed adsorption method. They also reported $1.0\cdot10^{-9}$ and $4.6\cdot10^{-9}$ cm^2 s^{-1} as the intraparticle BSA diffusivity, assuming the total BSA concentration to be the driving force of diffusion. Because, under the experimental conditions of these measurements, the slope of the isotherm chord is of the order of 100, the intraparticle diffusivity corresponding to D_e is of the order of 10^{-7} cm^2 s^{-1}. The values of D_e shown in Fig. 4a and b and the ratio D_e/D_m determined above are comparable to these literature data. It is thus likely that the estimates of D_e derived in this study are correct.

In Fig. 3, $F/(Kk_{m,L})$ was plotted against $1/K$ to estimate k_{ads}. It was assumed that the contribution of intraparticle diffusion was negligibly small when K is infinite. As shown in Fig. 4a and b, the value of D_e increases rapidly with decreasing C in the low concentration range, suggesting that the assumption is indeed valid. This validates the procedure of estimating k_{ads} from the plot of $F/(Kk_{m,L})$ versus $1/K$.

In this study, we assumed the parallelism of the contributions of pore and surface diffusion to intraparticle diffusion (Eq. (16)). This equation suggests that D_e tends toward D_p as K (namely, K_a) tends toward zero. In Fig. 5, D_e is plotted against K. From the intercept of the straight lines, D_p was estimated at $1.25\cdot10^{-7}$ cm^2 s^{-1} for the Resource-Q column and $1.23\cdot10^{-8}$ cm^2 s^{-1} for the TSK column. As explained earlier, the error made on D_e is estimated to less than ±10% for both the Resource-Q and TSK columns. From Eq. (16), it is likely that the same error is made on D_p and on D_e. The value of D_p on the TSK column is one tenth of that on the Resource-Q column. This is another reason for the rate of mass transfer on the TSK column being smaller than on the Resource-Q one. The difference is probably due to different shapes and sizes of the micropores. More detailed studies are needed to clarify the correlation between structural properties of the anion exchanger and mass transfer rate of proteins in the packing material.

In most of the previous publications, the contribution of pore diffusion to intraparticle diffusion was not separated from that of surface diffusion. The value of D_p was not determined. Yoshida et al. [16] reported D_p of BSA in the chitosan particles as $1.0\cdot10^{-7}$ cm^2 s^{-1} and $2.7\cdot10^{-7}$ cm^2 s^{-1} at zero surface coverage. The D_p value of BSA calculated for the Resource-Q column is comparable with those reported by Yoshida et al. [16]. The ratio D_p/D_m (diffusibility) for BSA is 0.21 on the Resource-Q column and 0.021 on the TSK column. It was experimentally confirmed that D_p is between 3- and 30-times smaller than D_m for typical chromatography packing materials [1]. The diffusibility observed in this study is also similar to previous observations. In conclusion, appropriate values of D_p seem to be derived from the analysis of the correlation between D_e and K illustrated in Fig. 5.

4.4. Estimation of surface diffusion coefficient

At this stage, D_s may be derived from the experimental values of $k_{m,L}$ since the other kinetic parameters, e.g., D_L, k_f, D_p, and k_{ads} in Eqs. (16) and (20), are known. The error made on estimate of D_s is close to ±10% because D_e and D_p on the Resource-Q and the TSK columns were estimated with an error

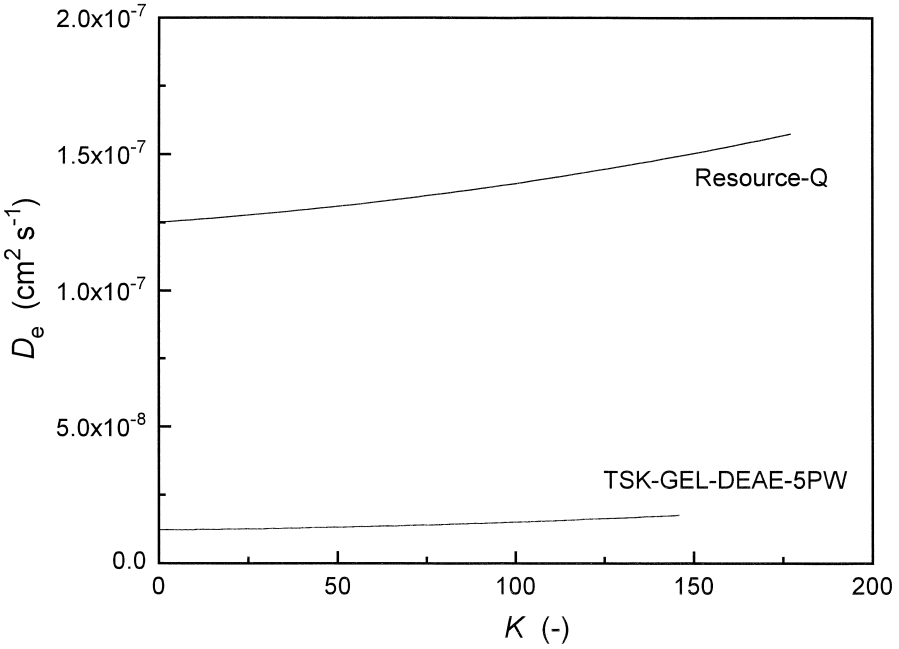

Fig. 5. Correlation between D_e and K for the estimation of D_p.

smaller than ±10%, as explained earlier, and D_e and D_p exhibit the same trends in their variations. For instance, if the estimate of D_e is larger than the true value, the resultant D_p calculated from the intercept in Fig. 5 is probably also larger than the true value. Fig. 6a illustrates the dependence of D_s of BSA on its concentration in the Resource-Q column (solid circle). Although the data in Fig. 6a are slightly scattered, D_s clearly increases with increasing concentration of BSA. D_s increases nearly 15-fold when C increases from infinite dilution to 2 mg ml^{-1}.

In this study, D_p was derived from D_m using Eq. (17). In order to confirm the validity of the values of D_s obtained, it was also calculated using another correlation between D_p and D_m [40,45].

$$D_p = \epsilon_p^2 D_m \quad (26)$$

The values of D_s so obtained are also reported in Fig. 6a (solid triangle). Although somewhat smaller than those obtained by the first correlation, they are quite comparable. The difference between them is smaller than ca. 20%.

Although the data were more dispersed, essentially the same results were obtained for the TSK column (Fig. 6b). D_s shows a positive concentration dependence. As described in the original papers [25,26], $k_{m,L}$ was determined by fitting experimental breakthrough curves to breakthrough curves calculated with a value of $k_{m,L}$ and the equilibrium isotherm which was determined separately. The accuracy of $k_{m,L}$ depends on that of the equilibrium isotherm. The error made on the equilibrium data is relatively large at low concentrations because of the steep rise shown in Fig. 1. This could explain the winding profile of the data points at low concentrations in Fig. 6b. It remains likely, however, that D_s increases with increasing BSA concentration. Tilton et al. [46] measured the lateral mobility of eosin isothiocyanate-labeled BSA on two different adsorbents, poly(methylmethacrylate) and poly(dimethylsiloxane). They reported $D_s = 1.2 \cdot 10^{-9}$ cm^2 s^{-1} and $2.6 \cdot 10^{-9}$ cm^2 s^{-1} for the former and the latter, respectively. Yoshida et al. [16] also reported D_s for BSA on chitosan as $4.7 \cdot 10^{-10}$ cm^2 s^{-1} and $2.4 \cdot 10^{-9}$ cm^2 s^{-1} at infinite dilution. The values of D_s in Fig. 6a

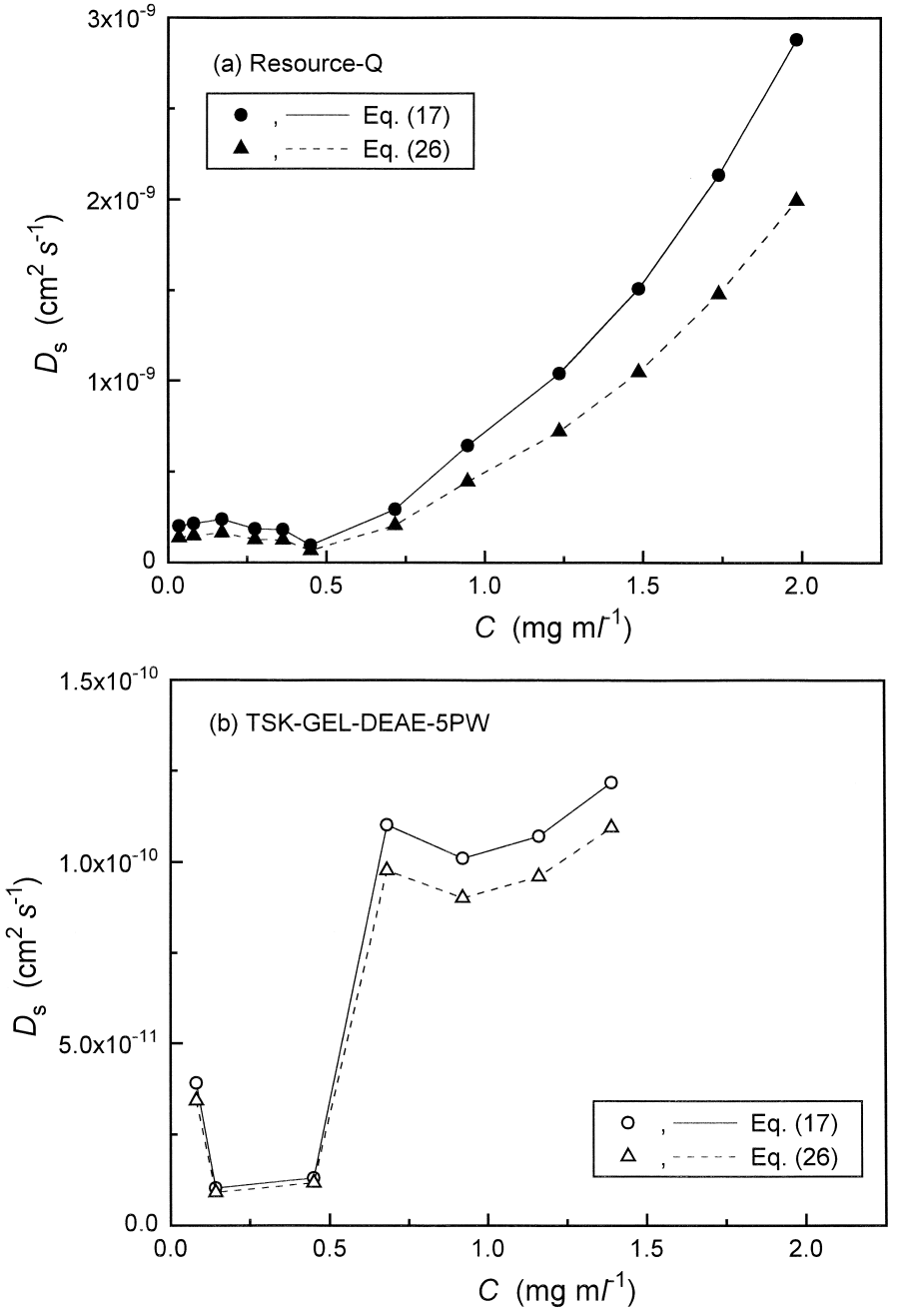

Fig. 6. Concentration dependence of D_s of BSA. (a) Resource-Q, (b) TSK-GEL-DEAE-5PW.

and b are comparable to these data, suggesting that appropriate values of D_s are probably obtained.

4.5. Comparison of the contribution of pore and surface diffusion to intraparticle diffusion

Fig. 4a and b show the contributions of pore and surface diffusion to intraparticle diffusion. For both columns, the correlations are very similar. As described above, D_p is assumed to be independent of C. The difference between D_e (solid circle) and D_p (open circle) corresponds to the contribution of surface diffusion (open triangle). The concentration dependence of the contribution of surface diffusion is explained by the similar dependences of K_a and D_s as described in Eq. (16). Fig. 7 illustrates the correlation between K_a and C.

At low concentrations, the contribution of surface diffusion is relatively large. However, it decreases steeply with increasing BSA concentration between 0 and 0.25 mg ml^{-1}. As predicted from Eq. (16) and Fig. 7, this decrease of the contribution of surface diffusion seems mainly due to the like variation of K_a. Around the minimum of D_e, the contribution of surface diffusion is relatively small. As described in Fig. 5, D_p was estimated from the intercept of the plot between D_e and K. In the concentration range around the minimum of D_e, the variation of the contribution of surface diffusion has little influence on the determination of D_p because it is small. As previously explained, it seems that appropriate values of D_p are obtained. On the other hand, at high concentrations, the coefficient of the second term of the RHS of Eq. (16), $(1-\epsilon_p)K_a$, decreases with increasing C, as illustrated in Fig. 7. However, D_e increases with increasing C or is constant at $C>$ca. 0.5 mg ml^{-1}. The dependence of D_e on C of BSA can no longer be explained by considering the variations of K_a. It is rather due to the positive concentration dependence of D_s (Fig. 6a and b).

In this work, experimental results previously published concerning the mass transfer kinetics in nonlinear frontal analysis were analyzed on the basis of the assumption that k_m represented the contributions of the three known mass transfer processes, fluid-to-particle mass transfer, intraparticle diffusion, and adsorption/desorption, and that these three contributions were additive, in nonlinear as well as linear chromatography, as indicated in Eq. (15). Although there is no theoretical proof of the validity

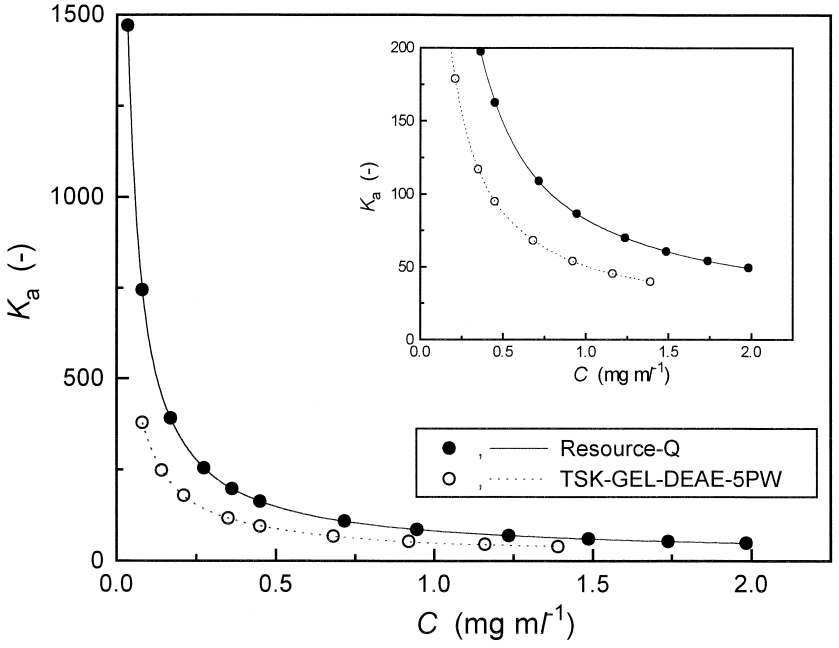

Fig. 7. Plot of K_a as a function of the BSA concentration. Inset: enlargement of the curve profile at low values of K_a.

of this assumption, the values of D_e, D_p and D_s reported and discussed above seem reasonable. This allows a further analysis of the experimental results.

4.6. Comparison of the contribution of the four mass transfer processes on the HETP

The following equation is derived from Eqs. (18), (18a) and (20).

$$H_{total} = \frac{2D_L}{u} + 2\cdot\left(\frac{K}{1+K}\right)^2\cdot\left[\frac{ud_p}{6Fk_f} + \frac{ud_p^2}{60FD_e} + \left(\frac{k_p}{1+k_p}\right)^2\cdot\frac{u}{Fk_{ads}}\right] \quad (27)$$

$$H_{total} = H_{ax} + H_f + H_d + H_r \quad (27a)$$

Eq. (27) is similar to Eq. (9). It correlates the total HETP (H_{total}) with the different kinetic parameters. As described above, the values of the kinetic parameters in Eqs. (16) and (20), i.e., D_L, k_f, D_e, D_p, D_s and k_{ads}, were obtained for different BSA concentrations. As described earlier, D_L was adequately derived for both the Resource-Q and TSK columns. Using Eq. (23), k_f was calculated with a reasonable accuracy. The other kinetic parameters, D_e, D_p, D_s and k_{ads}, were estimated with errors less than about ±10%. The contributions of the four terms in Eq. (27a) can then be calculated and compared with each other. Fig. 8a and b show the calculation results, which are different for the two anion exchangers. In Fig. 8a and b, the plots of H_{total} exhibit a maximum around $C = 0.25$–0.5 mg ml^{-1}. Eqs. (18) and (18a) suggest that this profile of H_{total} is due to the concentration dependence of both K (Fig. 7) and $k_{m,L}$ (Fig. 2). According to Eqs. (18) and (18a), H was probably estimated with an error less than about ±10% because the estimation errors on K and $k_{m,L}$ are respectively a few percent and ±10%, as described earlier. In Fig. 8a, the variation in H around the mean (about 0.14 cm) is about ±0.03 cm, larger than the error made in estimating H. It is probable that the profile of the plot of H in Fig. 8a is not much influenced by the error made on H.

In the case of the Resource-Q column (Fig. 8a), the contribution of intraparticle diffusion (H_d) is dominant. It varies between 63 and 75% of H_{total}, depending on the BSA concentration, while the contributions of other three mass transfer steps are almost equal and constant, irrespective of the BSA concentration. The lumped mass transfer rate coefficient ($k_{m,L}$) is correlated mainly with D_e. In such a case, H_{total} is approximately equal to $ud_p^2/(30FD_p)$ at $C = 0.5$ mg ml^{-1} because: (1) K is about 40 (Fig. 7) and (2) the contribution of surface diffusion to intraparticle diffusion is quite small (Fig. 4a). D_p is calculated as $1.0\cdot10^{-7}$ cm^2 s^{-1} from the parameters, i.e., $H_{total} = 0.17$ cm, $u = 0.067$ cm s^{-1}, $d_p = 1.5\cdot10^{-3}$ cm, and $F = 0.287$. The ratio D_p/D_m is about 0.17, in agreement with previous observations concerning this ratio, which supports the validity of the quantitative analysis of the kinetic data obtained in this study.

The linear dependence of $k_{m,L}$ illustrated in Fig. 2 is probably explained by the concentration dependence of D_s (Fig. 6a) because D_p is practically independent of the BSA concentration. If we assume that D_s is constant in the high concentration range, D_e would also be almost constant because K_a changes little. In this case, the contribution of H_d to H_{total} in Eq. (27), $2[K/(1+K)]^2(ud_p^2)/(60FD_e)$, becomes constant because the contributions of the other three mass transfer processes are almost constant. This suggests that, like H_d, H_{total} also is nearly constant at high concentrations because the other three mass transfer processes have almost constant and relatively small contributions. This prediction does not match the experimental results shown in Fig. 8a. H_{total} and H_d decrease with increasing C at high concentrations. This discrepancy results from the assumption that D_s is constant, irrespective of the BSA concentration. In conclusion, the decrease of H_{total} (Fig. 8a) and the increase of $k_{m,L}$ (Fig. 2) at high concentrations arises from the positive concentration dependence of D_s. This result shows that, although the contribution of surface diffusion to intraparticle diffusion is not always significant, as illustrated in Fig. 4a, surface diffusion provides the essential contribution to mass transfer kinetics in anion-exchange chromatography of BSA. The characteristic feature of surface diffusion should be analyzed in more detail for a better knowledge of the mass transfer kinetics in anion-exchange packing materials.

A different result was obtained for TSK (Fig. 8b).

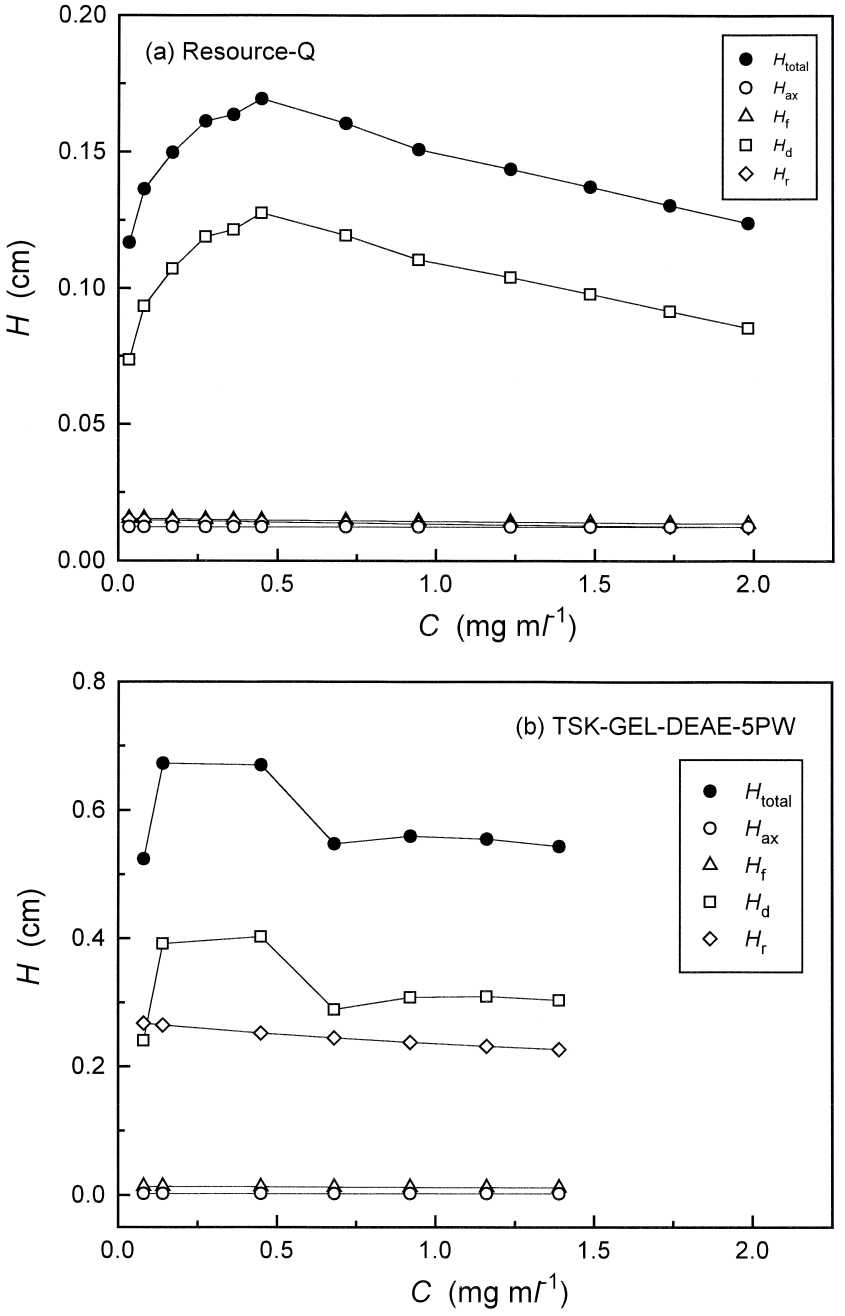

Fig. 8. Comparison of the contributions of the mass transfer resistance of each kinetic process in the column to the overall efficiency at different BSA concentrations. HETP: H_{total}, the overall column efficiency; H_{ax}, axial dispersion; H_f, fluid-to-particle mass transfer; H_d, intraparticle diffusion; H_r, adsorption/desorption. (a) Resource-Q, (b) TSK-GEL-DEAE-5PW.

The contributions to band broadening of intraparticle diffusion and adsorption/desorption are comparable and much larger than those of axial dispersion and the fluid-to-particle mass transfer resistance. The mass transfer properties of BSA inside the two anion exchangers are different. Although the ranges of H are different for the two columns, roughly similar profiles are observed for H_{total}, the overall index of column efficiency. The conclusions regarding the concentration dependence of H_{total} cannot be the same for the TSK and the Resource-Q column because the contribution of adsorption/desorption is relatively large in the case of the former column. However, D_s increases probably with increasing C in the TSK column (Fig. 6b). In the same way as for the Resource-Q column, a value of $=0.5$ mg ml^{-1} was calculated for the ratio D_p/D_m, hence $H_{total}=$ 0.65 cm, $u=0.048$ cm s^{-1}, $d_p=1.0\cdot10^{-3}$ cm, and $F=0.282$. Because the contribution of H_d to H_{total} was about 60%, a value of about $1.5\cdot10^{-8}$ cm^2 s^{-1} was estimated for D_p, approximately 40-times smaller than D_m of BSA, i.e., $6.0\cdot10^{-7}$ cm^2 s^{-1}. This value is also within the usual range of values of D_p/D_m obtained for liquid–solid systems.

4.7. Interpretation of the concentration dependence of D_s

The dependence of surface diffusion on both temperature and amount adsorbed was studied to characterize the migration mechanism in surface diffusion. Various models are available to explain these dependences [47]. The former is usually analyzed by the Arrhenius equation, assuming surface diffusion to be an activated process.

$$D_s = D_{s0} \exp\left(\frac{-E_s}{RT}\right) \tag{28}$$

where D_{s0} and E_s are the frequency factor and the activation energy of surface diffusion, respectively, and R the universal gas constant. Correlations were proposed between the thermodynamic properties of the phase equilibrium and of the mass transfer kinetics. For example, the following equation correlates E_s with the isosteric heat of adsorption (Q_{st}) using an entirely empirical parameter, α, which usually has a value between 0 and 1.

$$E_s = \alpha(-Q_s) \tag{29}$$

Combining Eqs. (28) and (29) gives the following equation

$$D_s = D_{s0} \exp\left[-\alpha\cdot\frac{(-Q_{st})}{RT}\right] \tag{30}$$

A number of experimental data on surface diffusion were analyzed with Eq. (30) [47].

There are also some models to explain the dependence of D_s on the amount adsorbed [47], for example, (1) the hopping model, (2) the heterogeneous surface model, (3) the Fick's law model, and (4) the surface pressure driving force model. In the hopping model, several equations were derived to correlate D_s and the surface coverage (θ) or ratio of q to the saturation capacity (q_s) [48–50]. In the heterogeneous surface model, a distribution of the adsorption energy is assumed. Because the adsorbate molecules are preferentially adsorbed on the higher energy adsorption sites, an increase in q tends to decrease the adsorption energy. Eq. (29) suggests that an increase in q is also accompanied with a reduction in E_s. As a consequence, D_s increases with increasing q, as predicted by Eqs. (28) and (30). When the heat of adsorption is proportional to q,

$$-Q_{st} = -Q_{st,0} + \beta q \tag{31}$$

where $Q_{st,0}$ is the isosteric heat of adsorption at zero surface coverage ($\theta=0$) and β a proportionality coefficient, which should be negative. Combining Eqs. (30) and (31) gives

$$D_s = D_{s0} \exp\left[-\alpha\cdot\frac{(-Q_{st,0})}{RT}\right] \exp\left(\frac{-\alpha\beta q}{RT}\right) \tag{32}$$

From Eq. (32), a linear correlation between ln D_s and q can be expected [51–53]. Friedrich et al. [53] concluded that the concentration dependence of D_s in liquid–solid adsorption of phenol and indole from aqueous solutions onto activated carbons was reasonably interpreted by Eq. (32). On the other hand, the concentration dependence of Q_{st} in the case of a Freundlich isotherm is written

$$-Q_{st} = -Q_{st,0} + \gamma(\ln q) \tag{33}$$

where γ is the slope of the linear correlation between $-Q_{st}$ and the logarithm of q, and is negative. By combining Eqs. (30) and (33), we obtain

$$D_s = D_{s0}\left[q\exp\left(\frac{-Q_{st,0}}{\gamma}\right)\right]^{\alpha n_F} \quad (34)$$

where n_F is the reciprocal of the exponent of the Freundlich isotherm and is equal to the ratio $-\gamma/(RT)$. Eq. (34) suggests a linear correlation between ln D_s and ln q. The slope of the linear correlation should be αn_F [54].

In the Fick's law model, the gradient of the surface concentration is usually taken as the driving force of surface diffusion. However, the concentration dependence of D_s is represented by the following equation in the chemical potential driving force model, in which the gradient of the chemical potential, not of the surface concentration, is regarded as the driving force [39,40].

$$D_s = D_{s,0}\cdot\left(\frac{\mathrm{dln}\,C}{\mathrm{dln}\,q}\right) \quad (35)$$

where $D_{s,0}$ is the value of D_s for $\theta=0$. The ratio dln C/dln q is the logarithmic slope of the adsorption isotherm, derived from the equilibrium isotherm. The value of dln C/dln q is equal to unity for a linear isotherm. For the Langmuir isotherm [$q=aC/(1+bC)$], dln C/dln q is equal to $1+bC$, suggesting the presence of a linear correlation between D_s and C.

In the surface pressure driving force model [55], the gradient of the surface pressure is assumed to be the driving force of surface diffusion. The following equation, similar to Eq. (35), is derived

$$D_s = \delta q\cdot\left(\frac{\mathrm{dln}\,C}{\mathrm{dln}\,q}\right) \quad (36)$$

where δ is a numerical parameter, assumed to be constant.

The various models described above suggest that the concentration dependence of D_s is related to changes in the magnitude of the interaction between the adsorbate molecules and the adsorbent surface and from in the driving force of surface diffusion, related with the adsorption isotherm. On the basis of this concept, we derived a more general formula for the concentration dependence of D_s in reversed-phase liquid chromatography [56].

As indicated in Fig. 1 and Eq. (1), the adsorption equilibrium of BSA in the two phase systems studied is accounted for by the modified bi-Langmuir equation, not by the Langmuir nor the Freundlich isotherm. The positive dependence of D_s on the BSA concentration observed in this study cannot be analyzed by correlations derived in the hopping model because the values of θ and q_s cannot be calculated from the modified bi-Langmuir isotherm. Eq. (34) cannot be applied either because it is derived from the Freundlich isotherm. So, we attempted to analyze the concentration dependence of D_s by using the other three models, the heterogeneous surface model, the chemical potential driving force model, and the surface pressure driving force model.

First, ln D_s was plotted against q (Fig. 9), according to Eq. (32) derived in the heterogeneous surface model. Although the low concentration data are somewhat scattered, it is likely that ln D_s increases almost linearly with increasing q at high concentrations. As mentioned above, the scatter of the data is probably due to errors of measurement of the equilibrium data at low concentrations. This suggests that the surface of the anion exchangers is heterogeneous and that there is an adsorption energy the distribution given by Eq. (31). As shown in Fig. 1 and Eq. (1), the adsorption equilibrium of BSA is given by the modified bi-Langmuir isotherm rather than the simple Langmuir one, suggesting that the surface of the anion exchangers is energetically heterogeneous. The results in Fig. 9 may be consistent with those predicted from the properties of the phase equilibrium of BSA. However, more detailed studies should be made to obtain a definite conclusion concerning the concentration dependence of D_s of BSA in anion-exchange chromatography.

Second, ln D_s was plotted against ln (dln C/dln q) in Fig. 10a, according to the chemical potential driving force model. No clear correlations were observed between ln D_s and ln (dln C/dln q). For the modified bi-Langmuir isotherm, dln C/dln q is given by

$$\frac{\mathrm{dln}\,C}{\mathrm{dln}\,q} = \frac{(1+b_1C)[a_1+a_2(1+b_1C)]}{a_1+a_2(1+b_1C)^2} \quad (37)$$

where a_1, b_1 and a_2 are the parameters of the

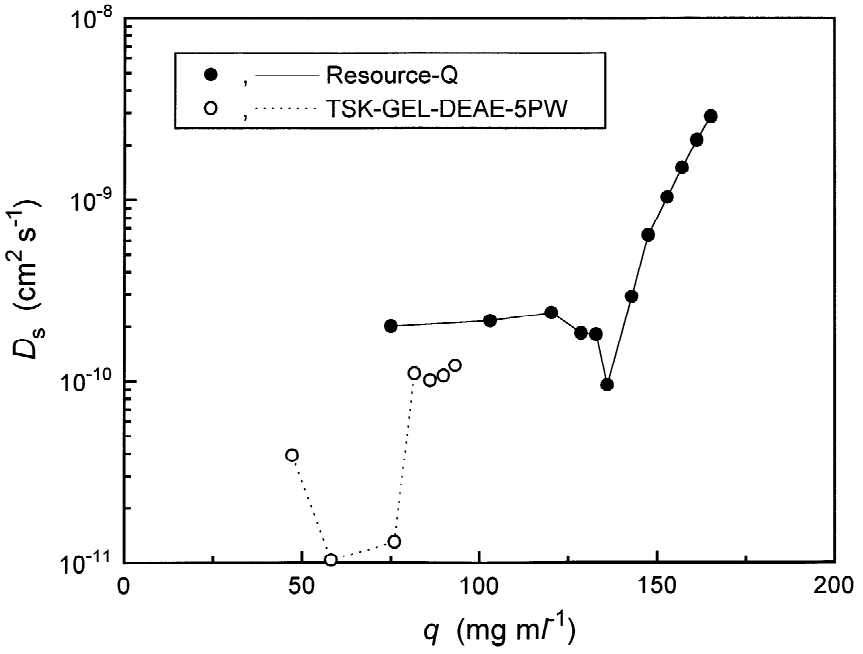

Fig. 9. Interpretation of the concentration dependence of D_s by the heterogeneous surface model.

modified bi-Langmuir isotherm (Eq. (1)). Fig. 10b shows plots of the values of dln C/dln q derived from Eq. (37) as a function of C for both columns. These plots go through a maximum. The trends of the plots in Fig. 10a is compatible with the presence of this maximum.

Finally, Fig. 11a and b show the same correlations between ln D_s and ln [q(dln C/dln q)] and that between q(dln C/dln q) and C, respectively. The value of q(dln C/dln q) was calculated by the following equation.

$$q \cdot \frac{\mathrm{dln}\, C}{\mathrm{dln}\, q} = \frac{C[a_1 + a_2(1 + b_1 C)]^2}{a_1 + a_2(1 + b_1 C)^2} \qquad (38)$$

The trends of the plots in Fig. 11a and b substantially resemble those in Fig. 10a and b, respectively. From the results in Figs. 10a and 11a, we may conclude that it is unlikely that the dependence of D_s of BSA on its concentration could be explained by the chemical potential driving force model or the surface pressure driving force model.

5. Conclusion

New information on the mass transfer of BSA on two anion-exchange chromatographic systems was derived from previous experimental results [25,26] using the most powerful approaches currently available. The main kinetic parameters, D_e, D_p, D_s and k_{ads}, which account for the different mass transfer processes active in the columns were calculated by analyzing the concentration dependence of the lumped mass transfer rate coefficient ($k_{m,L}$), assuming the validity of Eq. (15) in nonlinear frontal analysis. The values obtained were reasonable and compatible with other results reported previously. In conclusion, it was shown that, on the whole, D_s increases with increasing BSA concentration.

Then, the contributions of each mass transfer process, (1) axial dispersion, (2) the fluid-to-particle mass transfer resistance, (3) intraparticle diffusion, and (4) adsorption/desorption, to band broadening were calculated using these kinetic parameters. On the Resource-Q column, intraparticle diffusion was

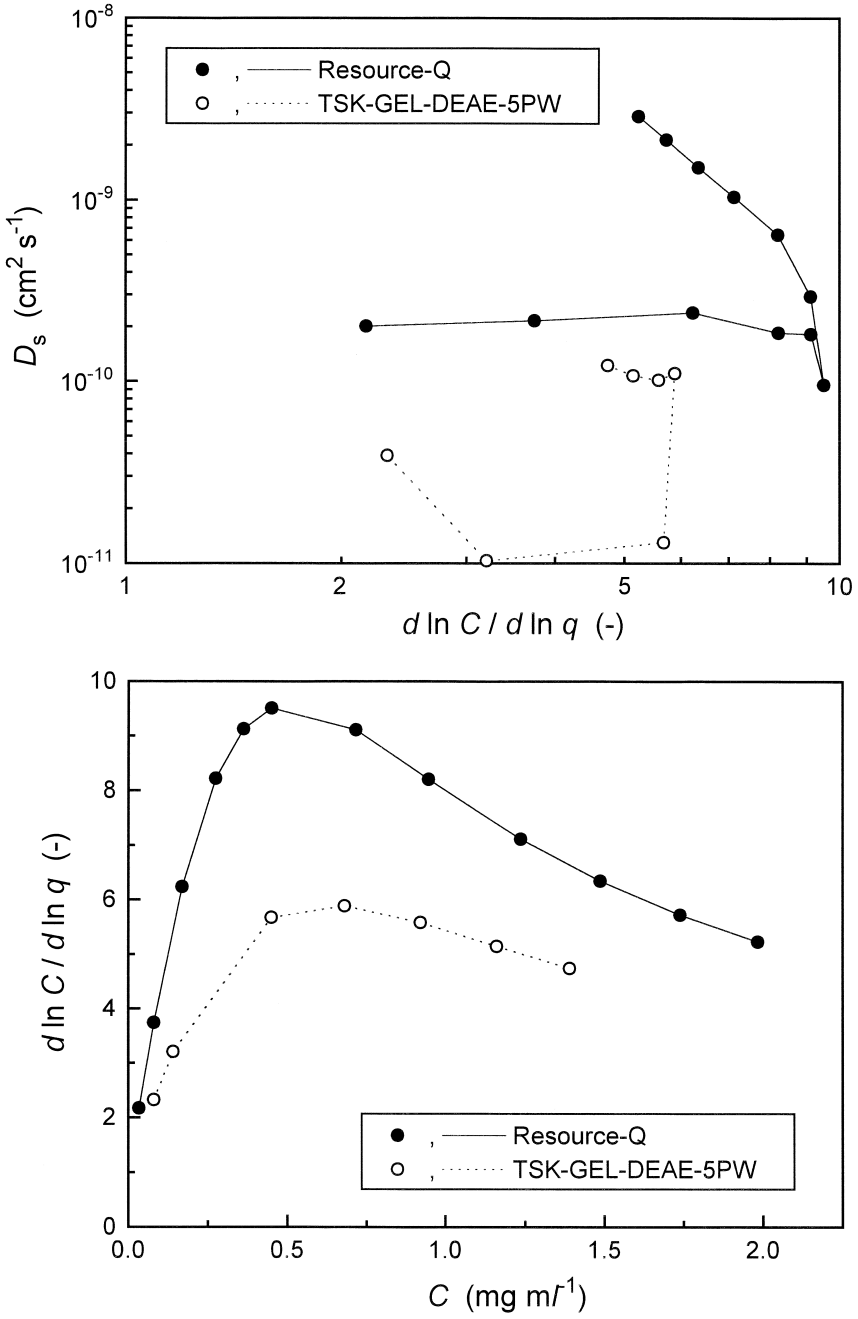

Fig. 10. Interpretation of the concentration dependence of D_s by the chemical potential driving force model. (a) Logarithmic plot of D_s against dln C/dln q, (b) plot of dln C/dln q as a function of the BSA concentration.

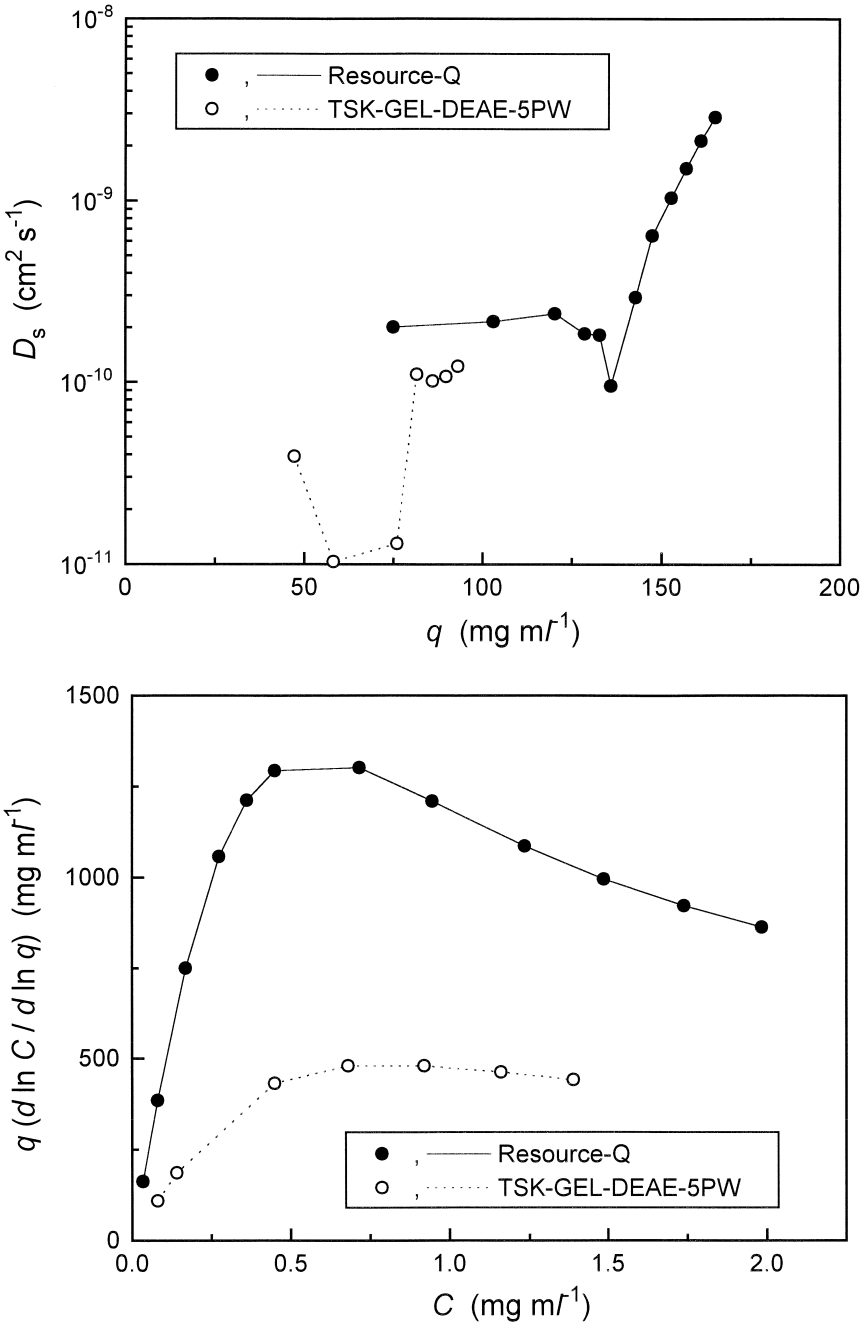

Fig. 11. Interpretation of the concentration dependence of D_s by the surface pressure driving force model. (a) Logarithmic plot of D_s against q(dln C/dln q), (b) plot of q(dln C/dln q) as a function of the BSA concentration.

the predominant source of mass transfer resistance, suggesting that surface diffusion has a major influence on the mass transfer characteristics of BSA and that the dependence of $k_{m,L}$ on the BSA concentration should be attributed to the positive concentration dependence of D_s. By contrast, on the TSK-GEL-DEAE-5PW column, the contribution of adsorption/desorption was also significant and almost equal to that of intraparticle diffusion, showing a difference between the intrinsic properties of the mass transfer kinetics inside the two anion-exchange stationary phases.

Finally, an attempt was made to explain the concentration dependence of D_s by applying some models. The concentration dependence of D_s seems due to an heterogeneous surface with an adsorption energy distribution of finite width. The kinetic properties of the individual mass transfer processes active in the column must be studied in more detail to elucidate the actual features of mass transfer kinetics in anion-exchange chromatography.

6. Symbols

a	Langmuir parameter (–)
a_1	Parameter of the bi-Langmuir isotherm (Eq. (1)) (–)
a_2	Parameter of the bi-Langmuir isotherm (Eq. (1)) (–)
b	Langmuir parameter (ml mg^{-1})
b_1	Parameter of the bi-Langmuir isotherm (Eq. (1)) (ml mg^{-1})
C	Concentration of the solute in the mobile phase (mg ml^{-1})
C_p	Concentration of the solute within the pores inside the particle (mg ml^{-1})
C_p^*	C_p in equilibrium with C_s (mg ml^{-1})
C_s	Concentration of the solute adsorbed on the stationary phase (mg ml^{-1})
C_s^*	C_s in equilibrium with C (mg ml^{-1})
C_0	Height of the rectangular injection pulse (mg ml^{-1})
d_p	Particle diameter (cm)
D_e	Intraparticle diffusivity (cm^2 s^{-1})
D_L	Axial dispersion coefficient (cm^2 s^{-1})
D_m	Molecular diffusivity (cm^2 s^{-1})
D_p	Pore diffusivity (cm^2 s^{-1})
D_s	Surface diffusion coefficient (cm^2 s^{-1})
D_{s0}	Frequency factor of surface diffusion (cm^2 s^{-1})
$D_{s,0}$	D_s at zero surface coverage (cm^2 s^{-1})
E_s	Activation energy of surface diffusion (kJ mol^{-1})
F	Phase ratio [$=(1-\epsilon_T)/\epsilon_T$)] (–)
H	Height equivalent to a theoretical plate (cm)
k_{ads}	Adsorption rate constant (s^{-1})
k_f	External mass transfer coefficient (cm s^{-1})
k_m	Mass transfer rate coefficient representing the contributions of fluid-to-particle mass transfer, intraparticle diffusion, and adsorption/desorption to band broadening (s^{-1})
$k_{m,L}$	Lumped mass transfer rate coefficient representing the contributions of axial dispersion, fluid-to-particle mass transfer, intraparticle diffusion, and adsorption/desorption to band broadening (s^{-1})
$k^0_{m,L}$	Parameter in Eq. (21) (s^{-1})
$k^1_{m,L}$	Parameter in Eq. (21) (ml mg^{-1} s^{-1})
k_p	Defined in Eq. (9b) (–)
k'_0	Retention factor at infinite dilution (–)
k_1	Defined in Eq. (9a) (–)
K	Partition coefficient in nonlinear chromatography [$=FK_a=F(\Delta q/\Delta C)$] (–)
K_a	Adsorption equilibrium constant (dq/dC or $\Delta q/\Delta C$) (–)
L	Column length (cm)
M	Molecular mass (–)
M_F	Mass flux of the solute from the bulk solution to the external surface of the stationary phase particle (mg cm^{-2} s^{-1})
n_F	Reciprocal of the exponent of the Freundlich isotherm (–)
N	Number of theoretical plates (–)
q	Concentration of the solute in the stationary phase (mg ml^{-1})
q_{av}	q averaged over the entire particle (mg ml^{-1})
q_s	Saturated amount adsorbed (mg ml^{-1})
Q_{st}	Isosteric heat of adsorption (kJ mol^{-1})
$Q_{st,0}$	Q_{st} at zero surface coverage (kJ mol^{-1})
r	Radial distance from the center of the particle (cm)
R	Gas constant (J mol^{-1} K^{-1})
Re	Reynolds number (–)

R_p Particle radius (cm)
Sc Schmidt number (–)
Sh Sherwood number (–)
St Stanton number (–)
t time (s)
t_p Width of the rectangular injection pulse (s)
T Absolute temperature (K)
u Average interstitial velocity of the mobile phase (cm s^{-1})
V_a Stationary phase volume inaccessible to the mobile phase (ml)
V_b Molar volume at the normal boiling point (cm^3 mol^{-1})
V_0 Hold-up volume of the column (ml)
z Longitudinal distance along the column (cm)

6.1. Greek symbols

α Ratio of E_s to $-Q_{st}$ (–)
α_A Association coefficient in Eq. (24) (–)
β Parameter in Eq. (31) (–)
δ Parameter in Eq. (36) (–)
ϵ Void fraction of the column (–)
ϵ_p Intraparticle porosity (–)
ϵ_T Total porosity of the column (–)
γ Parameter in Eq. (33) (–)
η Viscosity (Pa s)
θ Surface coverage (–)

6.2. Subscripts

ax Contribution of axial dispersion
B BSA
d Contribution of intraparticle diffusion
f Contribution of fluid-to-particle mass transfer
r Contribution of adsorption/desorption
s Unretained substance
sv Solvent
total Overall column

Acknowledgements

This work was supported in part by Grant CHE-97-01680 of the National Science Foundation and by the cooperative agreement between the University of Tennessee and the Oak Ridge National Laboratory.

References

[1] G. Guiochon, S. Golshan-Shirazi, A.M. Katti, Fundamentals of Preparative and Nonlinear Chromatography, Academic Press, Boston, MA, 1994.
[2] M. Verzele, C. Dewaele, Preparative High Performance Liquid Chromatography, TEC, Ghent, 1986.
[3] G. Guiochon, A.M. Katti, Chromatographia 24 (1987) 165.
[4] F.E. Regnier, J. Chromatogr. 418 (1987) 115.
[5] J.X. Huang, G. Guiochon, J. Chromatogr. 492 (1989) 431.
[6] The Handbook of Analysis and Purification of Peptides and Proteins by Chromatography, Vydac, Hesperia, CA, 1998.
[7] S.H. Chang, K.M. Gooding, F.E. Regnier, J. Chromatogr. 125 (1976) 103.
[8] E.E. Graham, C.F. Fook, AIChE J. 28 (1982) 245.
[9] Y. Kato, K. Nakamura, T. Hashimoto, J. Chromatogr. 245 (1982) 193.
[10] Y. Kato, K. Nakamura, T. Hashimoto, J. Chromatogr. 253 (1982) 219.
[11] H.S. Tsou, E.E. Graham, AIChE J. 31 (1985) 1959.
[12] E.A. James, D.D. Do, J. Chromatogr. 542 (1991) 19.
[13] J. Horvath, E. Boschetti, L. Guerrier, N. Cooke, J. Chromatogr. A 679 (1994) 11.
[14] A.E. Ivanov, V.P. Zubov, J. Chromatogr. A 673 (1994) 159.
[15] H. Yoshida, H. Nishihara, T. Kataoka, Biotechnol. Bioeng. 43 (1994) 1087.
[16] H. Yoshida, M. Yoshikawa, T. Kataoka, AIChE J. 40 (1994) 2034.
[17] S. Bouhallab, G. Henry, E. Boschetti, J. Chromatogr. A 724 (1996) 137.
[18] M.A. Fernandez, G. Carta, J. Chromatogr. A 746 (1996) 169.
[19] M.A. Fernandez, W.S. Laughinghouse, G. Carta, J. Chromatogr. A 746 (1996) 185.
[20] C.K. Colton, C.N. Satterfield, C.J. Lai, AIChE J. 21 (1975) 289.
[21] G.L. Skidmore, B.J. Horstmann, H.A. Chase, J. Chromatogr. 498 (1990) 113.
[22] I.H. Park, C.S. Johnson Jr., D.A. Gabriel, Macromolecules 23 (1990) 1548.
[23] J.X. Huang, J. Schudel G.Gu, G. Guiochon, J. Chromatogr. 504 (1990) 335.
[24] J.X. Huang, J. Schudel, G. Guiochon, J. Chromatogr. Sci. 29 (1991) 122.
[25] H. Guan-Sajonz, P. Sajonz, G. Zhong, G. Guiochon, Biotechnol. Prog. 12 (1996) 380.
[26] P. Sajonz, H. Guan-Sajonz, G. Zhong, G. Guiochon, Biotechnol. Prog. 13 (1997) 170.
[27] K. Miyabe, G. Guiochon, Biotechnol. Prog. 15 (1999) 740.
[28] P. Rearden, P. Sajonz, G. Guiochon, J. Chromatogr. A 813 (1998) 1.
[29] A. Seidel-Morgenstern, S.C. Jacobson, G. Guiochon, J. Chromatogr. 637 (1993) 19.

[30] P. Sajonz, M. Kele, G. Zhong, B. Sellergren, G. Guiochon, J. Chromatogr. A810 (1998) 1.
[31] B. Al-Duri, G. McKay, J. Chem. Techn. Biotechnol. 55 (1992) 245.
[32] S.J. Gibbs, A.S. Chu, E.N. Lightfoot, T.W. Root, J. Phys. Chem. 95 (1991) 467.
[33] K. Lederer, I. Amtmann, S. Vijayakumar, J. Billiani, J. Liq. Chromatogr. 13 (1990) 1849.
[34] W.H. Gallagher, C.K. Woodward, Biopolymer 28 (1989) 2001.
[35] R.L. Marlowe, H.E. Jackson, Spectrosc. Lett. 23 (1990) 1203.
[36] A.M. Katti, G. Guiochon, Adv. Chromatogr. 31 (1991) 1.
[37] J.J. van Deemter, F.J. Zuiderweg, A. Klinkenberg, Chem. Eng. Sci. 5 (1956) 271.
[38] L. Lapidus, N.R. Amundson, J. Phys. Chem. 56 (1952) 984.
[39] D.M. Ruthven, Principles of Adsorption and Adsorption Processes, Wiley, New York, 1984.
[40] M. Suzuki, Adsorption Engineering, Kodansha/Elsevier, Tokyo, 1990.
[41] E.J. Wilson, C.J. Geankopolis, Ind. Eng. Chem. Fundam. 5 (1966) 9.
[42] R.C. Reid, J.M. Prausnitz, T.K. Sherwood, The Properties of Gases and Liquids, McGraw-Hill, New York, 1977.
[43] R.E. Treybal, Mass-Transfer Operations, McGraw-Hill, New York, 1980.
[44] M.T. Tyn, T.W. Gusek, Biotechnol. Bioeng. 35 (1990) 327.
[45] N. Wakao, J.M. Smith, Chem. Eng. Sci. 17 (1962) 825.
[46] R.D. Tilton, C.R. Robertson, A.P. Gast, J. Colloid Interface Sci. 137 (1990) 192.
[47] A. Kapoor, R.T. Yang, C. Wong, Catal. Rev.-Sci. Eng. 31 (1989) 129.
[48] K. Higashi, H. Ito, J. Oishi, J. Japan Atom. Energy Soc. 5 (1963) 846.
[49] R.T. Yang, J.B. Fenn, G.L. Haller, AIChE J. 19 (1973) 1052.
[50] M. Okazaki, H. Tamon, R. Toei, AIChE J. 27 (1981) 262.
[51] I. Neretnieks, Chem. Eng. Sci. 31 (1976) 465.
[52] Y. Sudo, D.M. Misic, M. Suzuki, Chem. Eng. Sci. 33 (1978) 1287.
[53] M. Friedrich, A. Seidel, D. Gelbin, Chem. Eng. Process 24 (1988) 33.
[54] M. Suzuki, T. Fujii, AIChE J. 28 (1982) 380.
[55] E.R. Gilliland, R.F. Baddour, J.L. Russel, AIChE J. 4 (1958) 90.
[56] K. Miyabe, G. Guiochon, Adv. Chromatogr., (1999) in press.